International Journal of Applied Electromagnetics and Mechanics 55 (2017) 45–60
DOI 10.3233/JAE-160129
IOS Press

Effects of structure parameters on the static electromagnetic characteristics of high speed solenoid valves

Jianhui Zhao[a], Yong Shi[a,*], Leonid Grekhov[b] and Xiuzhen Ma[a]
[a]*School of Power and Energy Engineering, Harbin Engineering University, Harbin 150001, Heilongjiang, China*
[b]*School of Power Engineering, Bauman Moscow State Technical University, Moscow 115569, Russia*

Abstract. Numerical calculations of high speed solenoid valves (HSV) are performed to understand the effects of the driving current and structural parameters on electromagnetic energy conversion in HSV. The results show that the driving current plays a prominent role on the capability of electromagnetic energy conversion. The changes in the electromagnetic force are determined by the total magnetic reluctance and the range of the driving current. For large driving currents, the capability of electromagnetic energy conversion is not significantly influenced by the driving current and is only slightly affected by the working air-gap. The larger the driving current becomes, the smaller the increase of the electromagnetic force is with an increasing of the working air-gap. Within a certain range of driving currents, the armature thickness has positive effects on the capability of electromagnetic energy conversion, but the effects are not significant at large driving currents. At different driving currents, the effect of the number of coil turns on the electromagnetic force is mostly determined by the effects of the coil turns on the total magnetic flux and the total magnetic reluctance.

Keywords: Static electromagnetic characteristic, solenoid valve, common rail injection, driving current, working air-gap

1. Introduction

High pressure common rail systems have been applied widely because of their characteristics, such as their injection pressures independent of engine speed, injection timing, and flexible injection strategies. Engines that are equipped with high pressure common rail systems could potentially realize the design goals of high combustion efficiency and low emissions [1–4]. Injectors are key parts of high pressure common rail systems and directly affect the fluctuations of the fuel injection, the gas-liquid two-phase flow characteristics of the high pressure fuel in nozzles, the fuel atomization characteristics and the quality of gas/oil mixture [5–9]. HSVs are core control components of common rail injectors. The high dynamic response of HSVs can improve the control accuracy of the cycle's fuel injection quantity and timing.

Although both the electromagnetic characteristics and the armature's mass determine the dynamic response of an HSV, the former have a more significant impact. Numerous studies have investigated the

*Corresponding author: Yong Shi, School of Power and Energy Engineering, Harbin Engineering University, Harbin 150001, Heilongjiang, China. Tel.: + 86 045182568316; Fax: +86 045182518036; Email: sy.heu@hrbeu.edu.cn.

static electromagnetic characteristics of HSVs. Sun et al. [10], Topcu et al. [11], and Jaber [12] analyzed the effects of the driving current on the electromagnetic force of HSVs and found that the driving current has a significant influence on the electromagnetic energy conversion. Cheng et al. [13] studied the effects of Fe-based soft magnetic material on the magnetic field distribution and found that the material magnetism significantly affects the electromagnetic force of the HSV. Wang et al [14] experimentally determined that Al-Fe-based soft magnetic material could significantly reduce the material's magnetic reluctance and consequently improve the efficiency of electromagnetic energy conversion. Liu et al. [15] presented a 3D simulation and analyzed the magnetic-field distribution of a solenoid valve with different airgaps and contact surfaces, and eventually determined the optimum airgap and optimum shape of the contact surface. Miller et al. [16] studied the effects of the number of coil turns on the electromagnetic force of a fast pneumatic brake actuator, and Liu et al. [17] performed numerical calculations and determined the effects of the structural parameters on the static electromagnetic force of a solenoid valve applied in an electronic unit pump.

Based on the changes between the electromagnetic force and structural parameters, scholars have used several optimization algorithms to calculate the optimum structure of HSVs. Liu et al. [18] adopted CloudPSO for the structural design of a direct action solenoid valve. Shin et al. [19] used the response surface methodology to optimize the dynamic response of a high-speed solenoid valve based on ANSYS. Sefkat [20] set up two optimization criteria of volume minimization and energy consumption minimization and used them to optimize the parameters of HSVs. Lu et al. [21] optimized the time interval between the injections of HSVs based on an injection control strategy.

These previous studies showed that the static electromagnetic characteristics of an HSV are closely related to its structure and control parameters and especially to its driving current. A small driving current will lead to a lower electromagnetic force and will be unable to lift an armature, and a large driving current may cause an electromagnetic valve to reach magnetic saturation and thus reduce the efficiency of the electromagnetic energy conversion [10–12]. However, systematic and in-depth investigations of the effects of the driving current coupled with the structural parameters are rare. To provide valuable information about electromagnetic energy conversion in HSVs, a systematic investigation was conducted, and the effects of the driving current and essential structural parameters on the static electromagnetic force were numerically studied and analyzed.

2. Description of models and methodology

2.1. Numerical model and calculation setup

Most previous studies of electromagnetic energy conversion have been based on 3D computational fluid dynamics (CFD) software [13,17–19], which requires both sophisticated computer configurations and long computation times. These disadvantages are more significant in the detailed design phase of HSVs because of the large number of calculations. In addition, the working process of the HSV in a common rail injector involves nonlinear transient coupling between electromagnetism, mechanism and hydraulic power, and it is difficult for 3D CFDs to perform these transient coupled computations. In studying high pressure common rails, most scholars first modelled a one-dimensional electromagnetic submodel and then coupled it into a one-dimensional mathematical model of a high pressure common rail system [22–24]. Therefore, the electromagnetic model of HSVs is very important. In this investigation, based upon the principle of electromagnetic coupling, a mathematical model of HSVs that considers

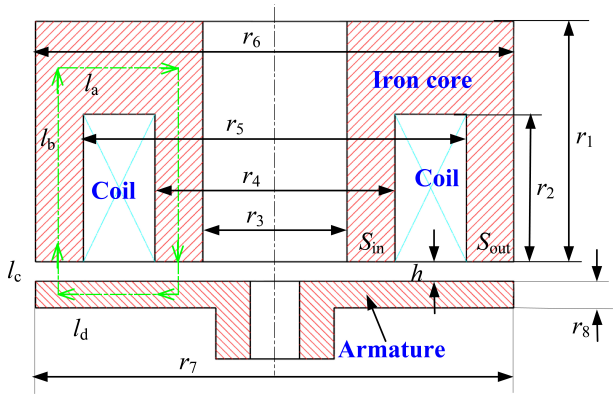

Fig. 1. The structural schematic of the HSV.

the phenomenon of electromagnetic saturation is deduced based upon the principle of electromagnetic coupling, and the effects of the electromagnetic energy conversion are studied. Figure 1 shows the structural diagram of an HSV for a common rail injector. The HSV is comprised of an iron core, a coil, and an armature.

The relationship between the total magnetic flux and the total magnetic reluctance in an HSV can be written as

$$\Phi = \frac{N \cdot I}{R_{total}} \tag{1}$$

Where Φ is the total magnetic flux, N is the number of coil turns, I is the driving current, and R_{total} is the total magnetic reluctance.

The total magnetic reluctance R_{total} can be written as

$$R_{total} = R_{gap1} + R_{gap2} + R_{arm} + R_{iron} \tag{2}$$

Where R_{gap1} is the corresponding air-gap of major pole, R_{gap2} is the corresponding air-gap of vice pole, R_{arm} is the magnetic reluctance of armature, and R_{iron} is the magnetic reluctance of iron coil. Respectively, the magnetic reluctance of each part can be written as follows.

$$R_{gap1} = \frac{l_c}{\mu_0 \cdot S_{in}} \tag{3}$$

$$R_{gap2} = \frac{l_c}{\mu_0 \cdot S_{out}} \tag{4}$$

$$R_{arm} = \frac{r_8}{2 \cdot \mu \cdot S_{in}} + \frac{r_8}{2 \cdot \mu \cdot S_{out}} + \frac{l_d}{\mu \cdot S''} \tag{5}$$

$$R_{iron} = \frac{l_b}{\mu \cdot S_{in}} + \frac{l_b}{\mu \cdot S_{out}} + \frac{l_a}{\mu \cdot S'} \tag{6}$$

where S_{in} is the effective cross-sectional area of major pole, S_{out} is the effective cross-sectional area of vice pole, l_c is the effective length of air-gap magnetic circuit, l_b is the effective length of magnetic circuit along the vertical direction inside iron core, l_a is the effective length of magnetic circuit along the horizontal direction inside iron core, l_d is the effective length of magnetic circuit along the horizontal direction inside armature, μ is the magnetic permeability of soft magnetic material, which is determined

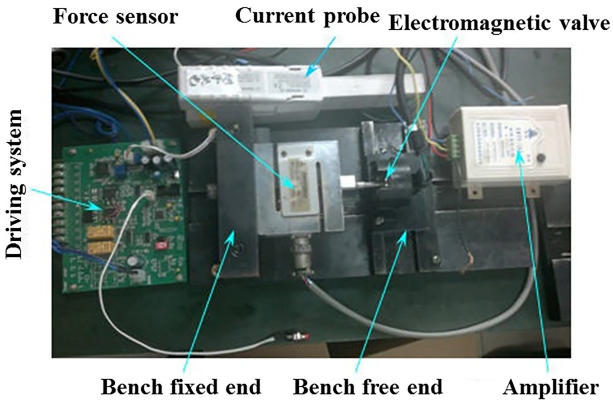

Fig. 2. The test bench of electromagnetic force for HSVs.

by the B-H curve, S'' is the corresponding effective cross-sectional area of l_d inside armature, and S' is the corresponding effective cross-sectional area of l_a inside armature.

The average magnetic circuit length and corresponding effective cross-sectional area of each part can be expressed as follows.

$$l_b = \frac{r_1 + r_2}{2} \tag{7}$$

$$l_a = \frac{r_5 + r_6 - r_3 - r_4}{4} \tag{8}$$

$$l_{\mathrm{d}} = l_{\mathrm{b}} \tag{9}$$

$$l_c = h \tag{10}$$

$$S' = \pi \cdot (r_1 - r_2) \cdot \frac{r_5 + r_6 + r_3 + r_4}{4} \tag{11}$$

$$S'' = \pi \cdot r_8 \cdot \frac{r_5 + r_6 + r_3 + r_4}{4} \tag{12}$$

$$S_{in} = \frac{\pi}{4} \cdot (r_4^2 - r_3^2) \tag{13}$$

$$S_{out} = \frac{\pi}{4} \cdot (r_6^2 - r_5^2) \tag{14}$$

Finally, the electromagnetic force of the HSV can be expressed as

$$F_{mag} = \frac{1}{2}\frac{\phi^2}{\mu_0 \cdot S_{in}} + \frac{1}{2}\frac{\phi^2}{\mu_0 \cdot S_{out}} \tag{15}$$

2.2. Validation of the mathematical model

To test and validate the accuracy of the electromagnetic model, a test bench is used to measure the static electromagnetic force (Fig. 2). The iron core of the HSV is placed at the free end of the bench, and the armature and force sensor are fixed at the fixed end. The height of the free end is adjusted to keep the axes of the iron core and the armature at the same horizontal level. The value of the working air-gap of the HSV can be changed by adjusting the distance between the free end and the fixed end. The driving current of the HSV is controlled by a power amplifier. The current is measured using a current

Table 1
The specifications of main sensors

Equipment	Force sensor	Current probe
Type	CZLYB-3	1146 A
Producer	Chengdu Xingpu transducer Co., Ltd.	Agilent technology
Measurement range	$0 \sim 500$ N	$1 \sim 100$ A
Measurement accuracy	$\leqslant \pm 0.05\%$	$\leqslant \pm 2\%$

Table 2
The detailed settings of the one-dimensional calculation

Parameters	Reference value
Height r1 (mm)	13.7
Diameter r6 (mm)	20.4
Diameter of hole r3(mm)	7
B-H curve of soft material	B-H curve in Fig. 3
Coil turns N (−)	52
Height r2 (mm)	7.6
Inside diameter r4 (mm)	12
Outside diameter r5 (mm)	17.7
Thickness r8 (mm)	1.8
Diameter r7 (mm)	20
Working air-gap h (mm)	0.1; 0.12
Driving current I (A)	$1 \sim 18$

probe. The armature will be attracted towards the iron core when the coil is energized. A force sensor generates a weak voltage signal, which passes through a high-precision amplifier to denote the value of the electromagnetic force in the axial direction. Table 1 shows the specifications of the main sensors. By changing the air-gap and the driving current, the data of static electromagnetic force were measured on the test bench. Subsequently, the static electromagnetic characteristics of the HSV were obtained.

Table 2 shows the detailed structural parameters of the HSV, and Fig. 3 shows the B-H curve of the soft magnetic material. The electromagnetic forces at different driving currents are calculated by combining Eqs (1)–(15) and the B-H curve.

Figure 4 shows comparisons between the simulated and experimental results of the electromagnetic force at various driving currents and working air gaps. For working air-gaps of 0.1 mm and 0.12 mm, the simulated and experimental results are consistent at different driving currents. These results demonstrate that the proposed electromagnetic model of the HSV is reasonable and can be used to predict the electromagnetic force of an HSV with acceptable accuracy. Therefore, based on the validated electromagnetic model of the electromagnetic force, the effects of the structural parameters on the electromagnetic energy conversion are studied at different driving currents.

3. Results and discussions

3.1. Influence of the driving current

The effects of the driving current I on the capability of electromagnetic energy conversion can be analyzed using the test data of the static electromagnetic force (Fig. 4). Figure 5 shows the variation of the electromagnetic force with increasing driving current. When I increases from 1 A to 18 A, the electromagnetic force first increases rapidly, reaches a maximum value at a driving current of 4 A, and

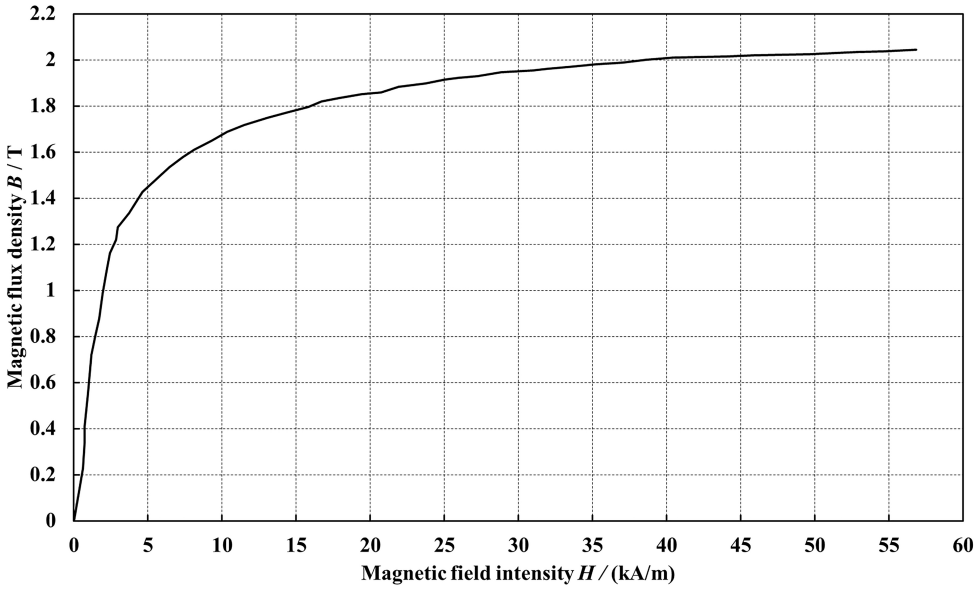

Fig. 3. The B-H curve of the iron core and armature.

then decreases. When $I < 4$ A, with increasing I, the increase of the electromagnetic force at the air-gap of 0.1 mm always greater than that at the air-gap of 0.12 mm. When $I > 4$ A, the two curves nearly overlap, and the increment of the electromagnetic force with increasing I gradually decreases. The phenomena can be explained with the B-H curve of the iron core and armature. The variation of the electromagnetic force is actually determined by both the total magnetic reluctance R_{total} and I, each of which makes a different contribution to the variation at different values of I.

Figure 6 shows that when $I < 4$ A, at different working air-gaps, the total magnetic reluctance increases with increasing I, but its growth is so small that the electromagnetic force does not decrease significantly. Therefore, for this case, the driving current plays a major role in the increase of the electromagnetic force, and thus the electromagnetic force increases rapidly with increasing driving current. When $I > 4$ A, with increasing I, although the positive effect induced by the rise of the total magnetic flux is greater than the negative effect caused by the increase of the total magnetic reluctance, the negative effect increases more rapidly. Consequently, the effects of the total magnetic reluctance on the electromagnetic force increase continuously, and the increase of the electromagnetic force decreases gradually with increasing I.

Figure 6 also shows that when $I < 4$ A, the smaller the working air-gap is, the smaller the total magnetic reluctance becomes. When the total magnetic flux is constant ($I =$ constant), a smaller total magnetic reluctance means a greater electromagnetic force. Therefore, for this case, with increasing I, the increase of the electromagnetic force at the working air-gap of 0.10 mm is always greater than that at the working air-gap of 0.12 mm (Fig. 5). When $I > 4$ A, increasing I will cause premature saturation in the HSV, and the magnetic reluctance of the soft magnetic material will become a decisive factor in restricting the variation of the total magnetic reluctance, which causes the changes of the total magnetic reluctance at different working air-gaps to be the same with increasing I (Fig. 6). Therefore, it can be surmised that when $I > 4$ A, the electromagnetic forces with different working air-gaps will increase at the same rate with increasing I.

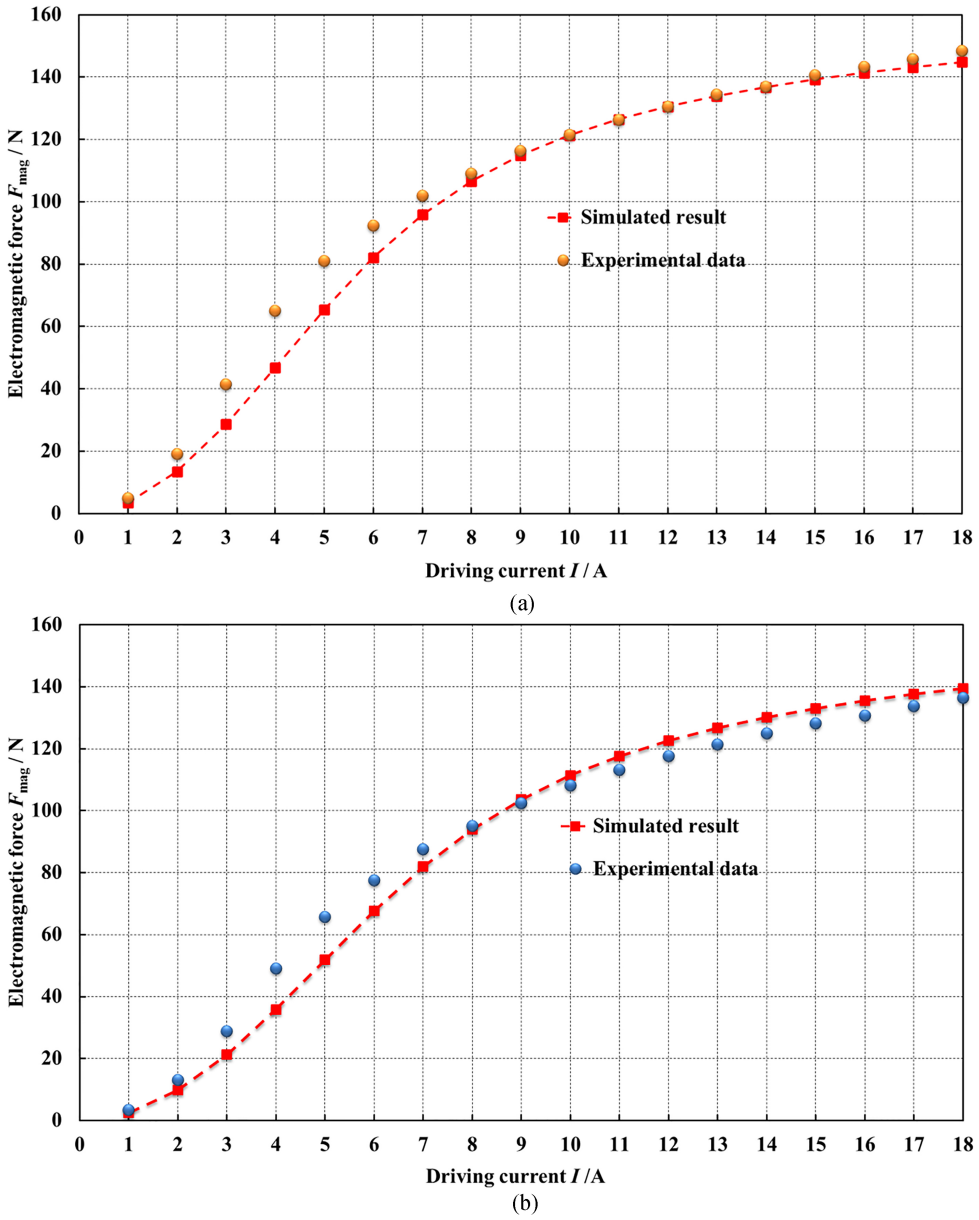

Fig. 4. Comparison between simulated and experimental results of the electromagnetic force at different air-gaps: (a) air-gap of 0.1 mm; (b) air-gap of 0.12 mm.

3.2. Influence of the working air-gap

Figure 7 shows that at different values of I, the electromagnetic force decreases with an increasing of the working air-gap, and the rate of decrease is affected by the value of I. The larger I becomes, the smaller the rate is. As the working air-gap increases from 0.4 mm to 1.6 mm, the electromagnetic force decreases by approximately 70 N for $I = 5$ A and by approximately 5 N for $I = 20$ A. This difference occurs because I and the working air-gap both have significant effects on the variation of

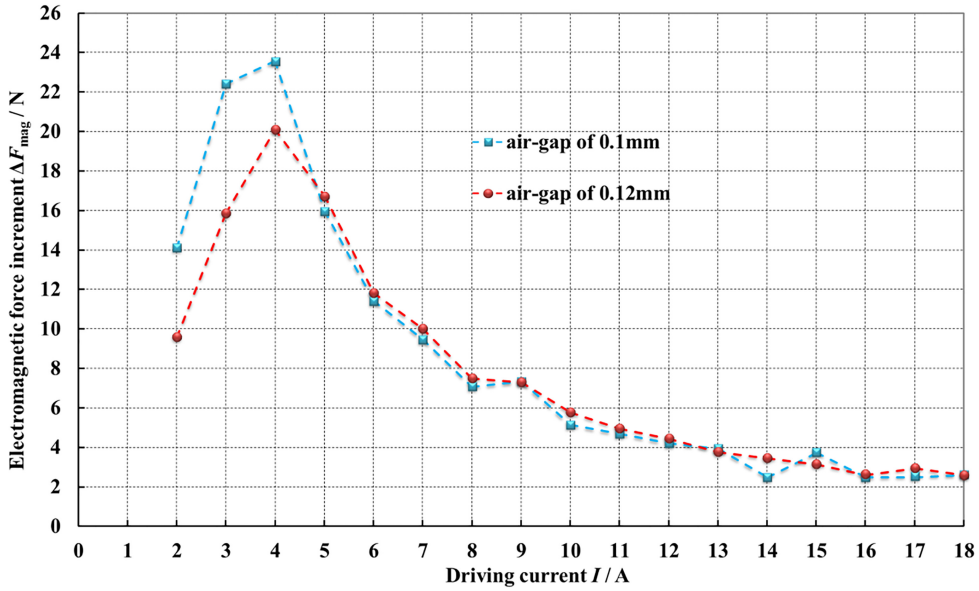

Fig. 5. Influence of the driving current on the electromagnetic force increment at different working air-gaps.

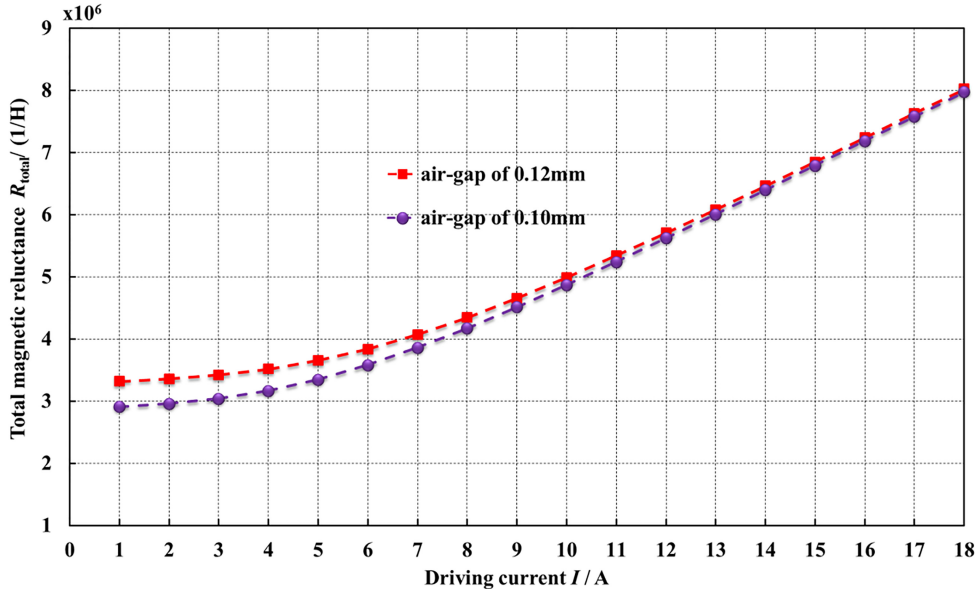

Fig. 6. Influence of driving current on total magnetic reluctance at different working air-gaps.

the total magnetic reluctance. Too large current or small working air-gap will lead to the saturation of magnetic circuit. Figure 8 shows that at different values of I, the total magnetic reluctance increases with an increase of the working air-gap. When the total magnetic flux is constant, the electromagnetic force decreases with increasing total magnetic reluctance.

At different values of I, the changes in the total magnetic reluctance are also different. When $I = 5$ A, the total magnetic reluctance increases significantly with increases of the working air-gap, which causes

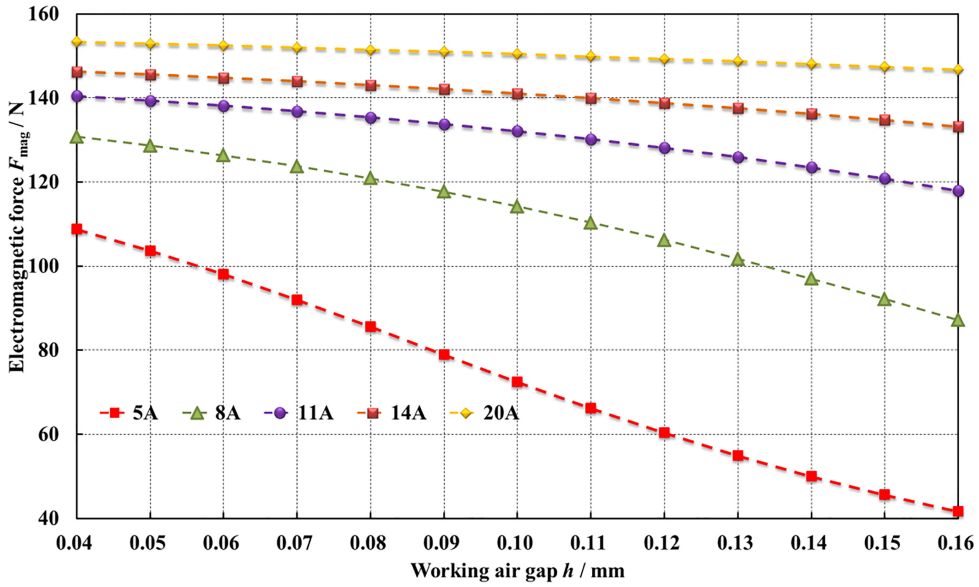

Fig. 7. Influence of h on the electromagnetic force at different driving currents.

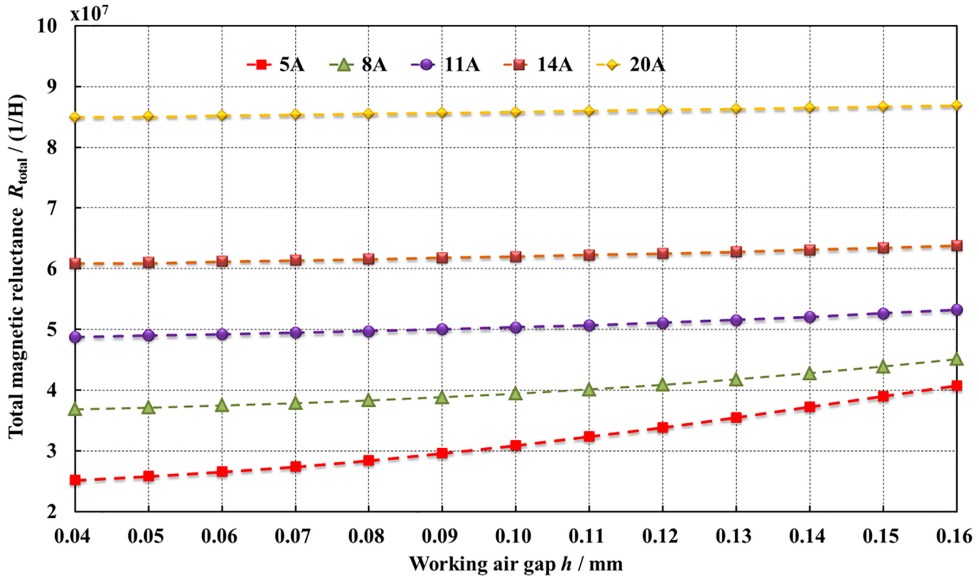

Fig. 8. Influence of h on the total magnetic reluctance at different driving currents.

a decrease of the electromagnetic force. However, when I increases from 5.0 A to 20 A, the growth rate of the total magnetic reluctance decreases with increasing I, although the total magnetic reluctance still increases. Therefore, if I is small, the capability of electromagnetic energy conversion in the HSV will be significantly influenced by the working air-gap. But if I is large enough to lead to the magnetic saturation, the working air-gap has only a minor influence.

The working air-gap has direct effects on the air-gap's magnetic reluctance as well as the magnetic reluctance of the soft magnetic material in the HSV. In the case of constant structural parameters, the

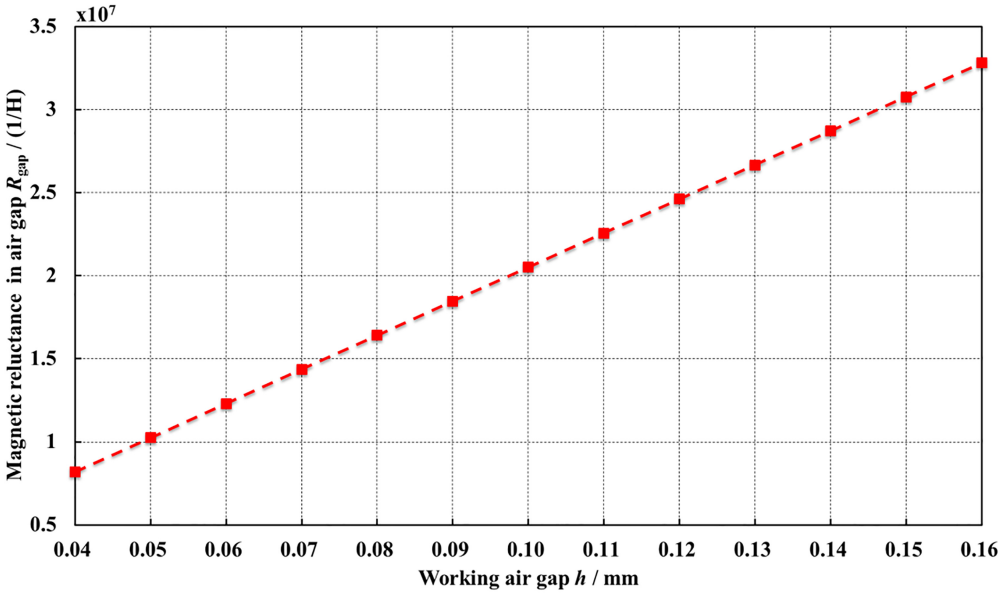

Fig. 9. Influence of h on the magnetic reluctance.

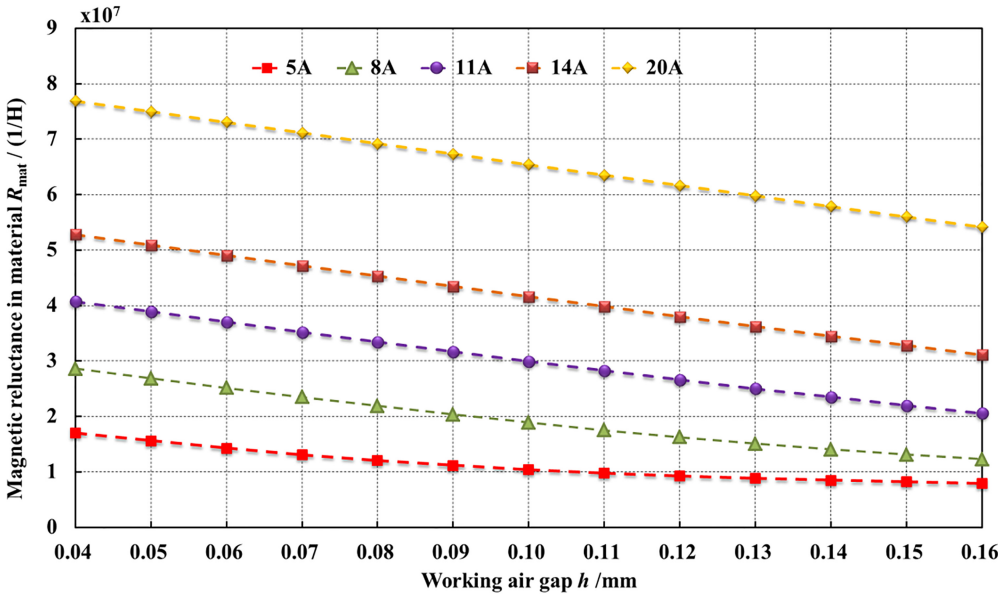

Fig. 10. Influence of h on the magnetic reluctance in material at different driving currents.

air-gap's magnetic reluctance increases linearly with an increase of the working air-gap regardless of the value of I. However, as shown in Fig. 8, with an increasing of the working air-gap, the increasing rate of the total magnetic reluctance is greater than that of the air-gap's magnetic reluctance (Fig. 9). Figure 8 also shows that the increasing rate of the total magnetic reluctance decreases with increasing driving current. This phenomenon is mainly attributed to the effects of the working air-gap on the magnetic reluctance of the soft magnetic material.

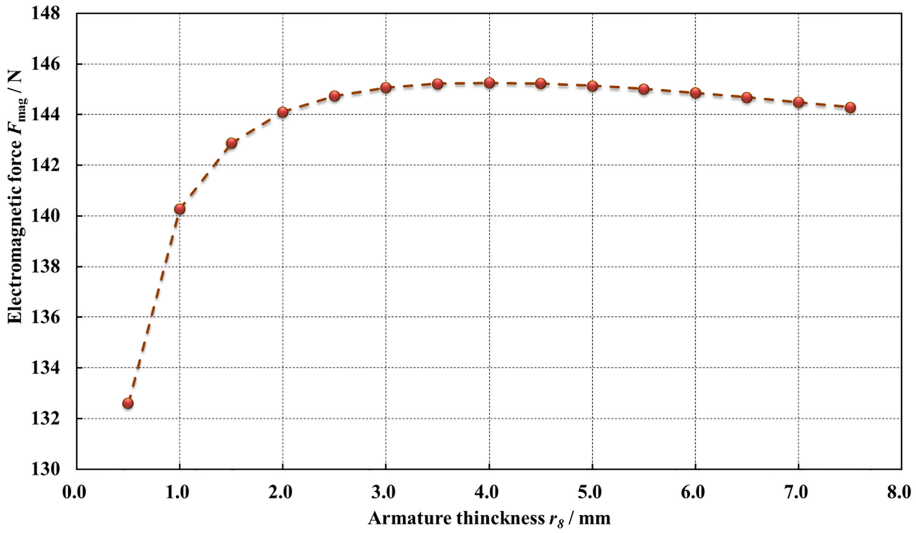

Fig. 11. Influence of r_8 on the electromagnetic force at $I = 15$ A.

Figure 10 clearly shows that at different values of I, the magnetic reluctance of the soft magnetic material decreases with an increasing of the working air-gap and that the rate of change increases with increasing I. At different values of I, the increase of the air-gap's magnetic reluctance is always greater than the reduction of the magnetic reluctance of the soft magnetic material with increases of the working air-gap, and the latter relies on the value of the driving current. When $I = 5$ A, the magnetic reluctance of the soft magnetic material decreases slowly with increases of the working air-gap, while the air-gap's magnetic reluctance rises sharply, which leads to rapid increases of the total magnetic reluctance. Therefore, if I is small, the total magnetic reluctance increases with an increase of the working air-gap, but its growth is less than that of the air-gap's magnetic reluctance. With an increase of I from 5 A to 20 A, although the air-gap's magnetic reluctance continues to increase substantially, the decrease of the magnetic reluctance of the soft magnetic material enhances gradually with increases of the working air-gap, which causes the reduction of the magnetic reluctance of the soft magnetic material to have more significant effects on the reduction of the total magnetic reluctance. Hence, the total magnetic reluctance of the HSV increases slowly with increasing working air-gap. It can be surmised that the capability of electromagnetic energy conversion is restricted by the magnetic saturation of the HSV.

3.3. Influence of the armature thickness

An increment of the armature thickness r_8 will increase the mean magnetic path length l_d, which will lead to an increase of the magnetic reluctance of the soft magnetic material. On the other hand, an increment of the armature thickness also causes an increment of the effective cross-sectional area S'' of the magnetic flux in the armature's radial direction, which consequently decreases the magnetic reluctance of the soft magnetic material. As shown in Fig. 10, with an increase of r_8 from 0.5 mm to 8 mm, the electromagnetic force first increases rapidly to a maximum value and then decreases slowly with the increment ofincreasing r_8. The increase of r_8 from 1 mm to 4 mm causes the increase of S'' to be more than that of l_d, and the competition between the two increases leads to an increase of the magnetic reluctance of the soft magnetic material with rising r_8. Therefore, when the total magnetic flux is constant, the electromagnetic force increases rapidly with increasing r_8 (Fig. 11). When r_8 is

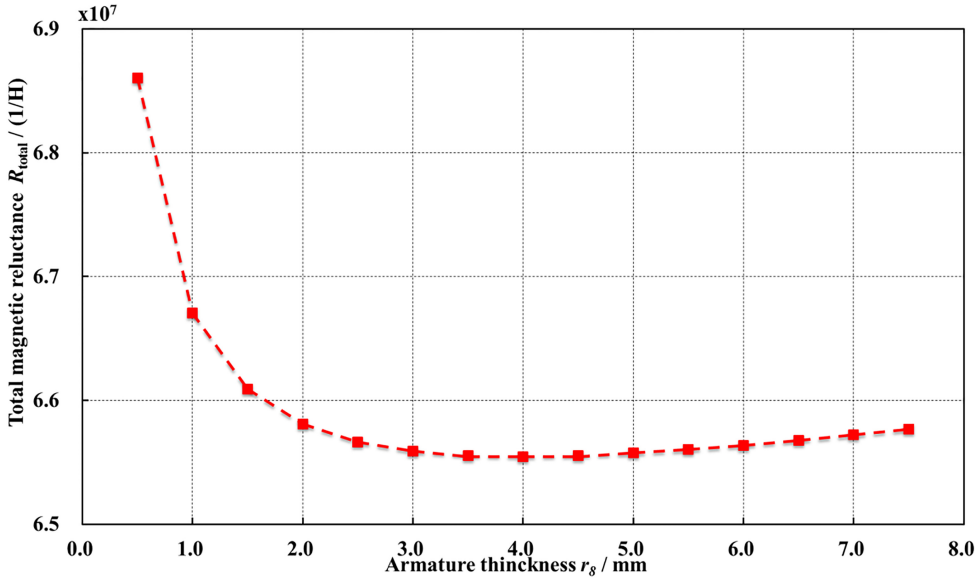

Fig. 12. Influence of r_8 on the total magnetic reluctance at $h = 0.1$ mm and $I = 15$ A.

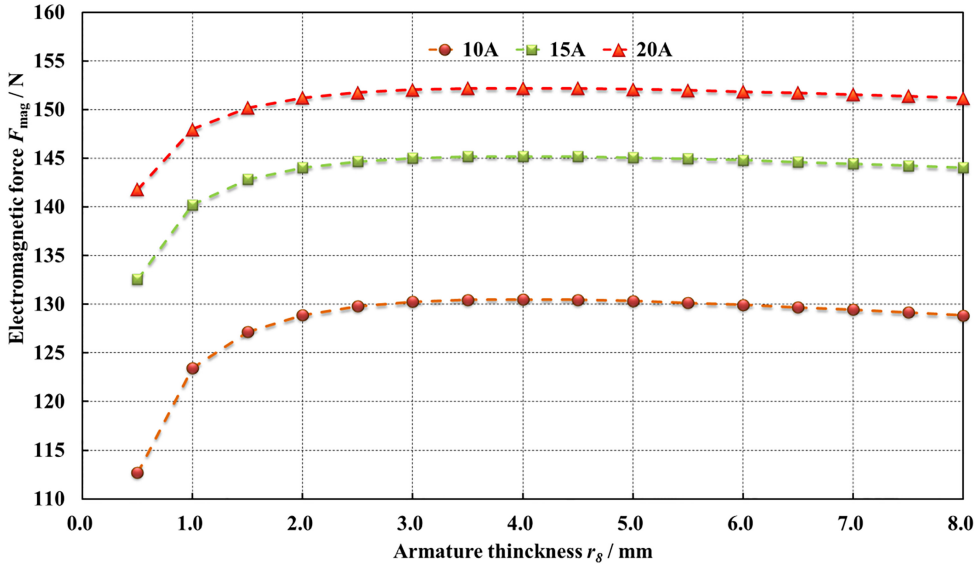

Fig. 13. Influence of r_8 on the electromagnetic force at different driving currents.

greater than 4 mm, with increasing r_8, the growth of l_d begins to be greater than that of S'', which causes a reduction of the total magnetic reluctance (Fig. 12) and eventually leads to a slight increase of the electromagnetic force with increasing r_8.

Figure 13 shows that at different values of I, the variations of the electromagnetic force with the working air-gap are different. With an increase of I from 10 A to 20 A, the larger the driving current is, the smaller the effects of r_8 on the electromagnetic force are. If I is small and its magnetic field is far from magnetic saturation, the increase of r_8 will decrease the total magnetic reluctance and increase

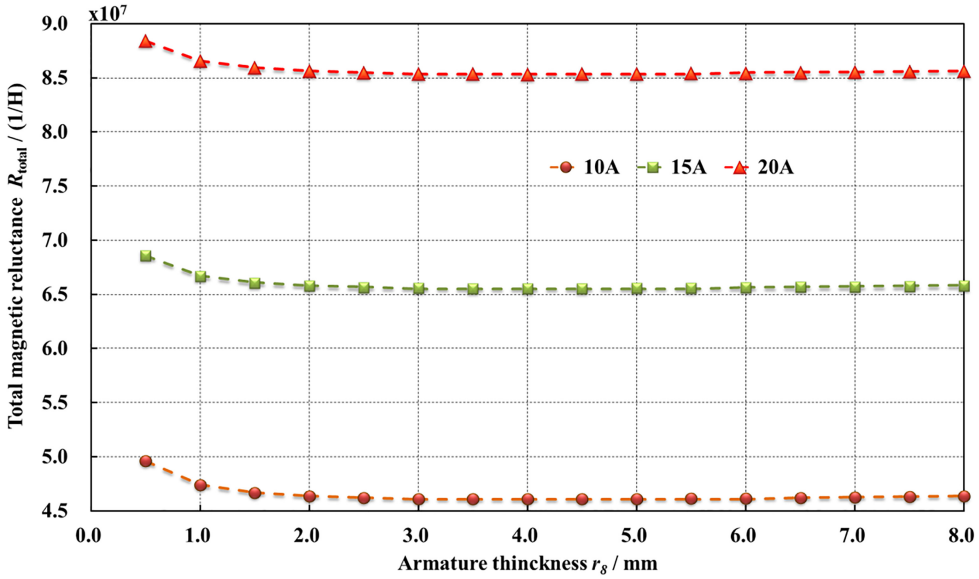

Fig. 14. Influence of r_8 on the total magnetic reluctance at different driving currents.

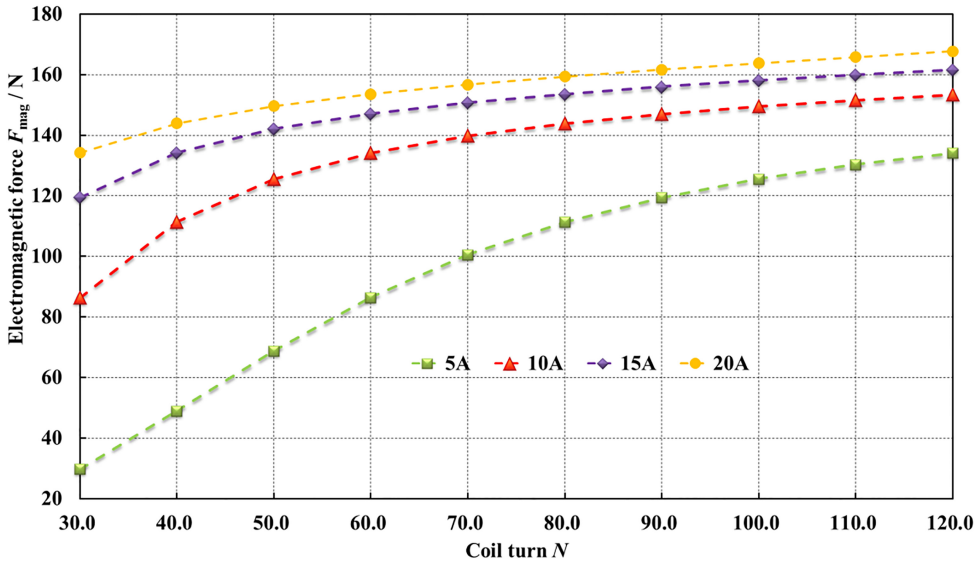

Fig. 15. Influence of N on the electromagnetic force at different driving currents.

the electromagnetic force significantly. However, if I is large and near magnetic saturation, the increase of r_8 cannot cause a significant reduction of the total magnetic reluctance (Fig. 14). Naturally, the electromagnetic force decreases slightly with an increase of r_8, and the rate of reduction is small. These results indicate that the positive effects of r_8 on the capability of electromagnetic energy conversion can be increased by increasing the current within a certain range, but it will be negatively affected by an excessively high current.

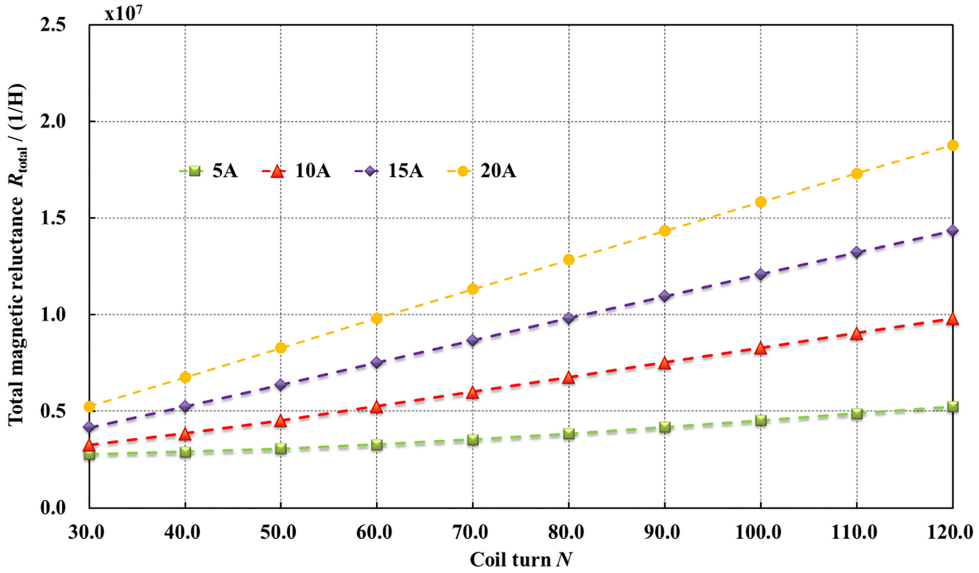

Fig. 16. Influence of N on the total magnetic reluctance at different driving currents.

3.4. Influence of the number of coil turns

Figure 15 shows that at different values of I, with an increase of the number of coil turns, the electromagnetic force of the HSV will increase by different amounts. The larger I, the smaller the increase of the electromagnetic force. On one hand, an increase in the number of coil turns N will increase the total magnetic flux Φ and lead to a higher electromagnetic force. On the other hand, the increase of N will increase the total magnetic reluctance and lead to a decrease of the electromagnetic force. Therefore, at different values of I, the effects of N on the electromagnetic force are determined by the effects of N on the magnetic flux and the magnetic reluctance.

At different values of I, with an increasing of N from 30 to 120, the total magnetic reluctance increases continually, but the growth of the total magnetic flux is always greater than that of the total magnetic reluctance. Figure 15 shows the increases of the electromagnetic force with increasing N at different values of I. Although the total magnetic flux plays a major role in the variation of the electromagnetic force, the role gradually decreases with increasing N because the effects of the total magnetic reluctance on the reduction of the electromagnetic force decrease.

Figure 16 shows that with an increasing of I from 5 A to 25 A, the total magnetic reluctance increases sharply. Although the increase of the total magnetic reluctance plays a major role in the increase of the electromagnetic force as N increases, the increase of I intensifies the effects of the total magneti reluctance on the reduction of the electromagnetic force. Figure 15 shows that the larger I is, the smaller the increase of the electromagnetic force becomes with increasing N.

4. Conclusions

A numerical method is used to analyse the effects of the structural parameters of an HSV on its capability of electromagnetic energy conversion at different currents. The main conclusions are as follows:

(1) The driving current plays a prominent role in the electromagnetic force of an HSV. Changes in the electromagnetic force with the driving current are determined by the ranges of the total magnetic reluctance and driving current. If the driving current is small, it is the main factor that changes the electromagnetic force. However, if the driving current is large, although the increase of the total magnetic flux is the main factor in the increase of the electromagnetic force, an increase of the total magnetic reluctance enhances the reduction of the electromagnetic force, which gradually weakens the effects of the driving current on the capability of electromagnetic energy conversion.
(2) The electromagnetic force will reduce with an increase of the working air-gap, and the reduction will decrease with increases of the driving current. For the case of a large driving current, the efficiency of electromagnetic energy conversion is slightly influenced by the working air-gap. Changes in the working air-gap can influence the air-gap's magnetic reluctance as well as the magnetic reluctance of the soft magnetic material.
(3) The effects of the armature thickness on the electromagnetic energy conversion of the HSV are determined by the driving current. Within a certain range of driving currents, an increase of the armature thickness increases the capability of electromagnetic energy conversion. However, in the case of a large driving current, the armature thickness plays a minor role in the capability of electromagnetic energy conversion.
(4) The electromagnetic force will increase with an increasing in the number of coil turns, but its growth is determined by the driving current. The effects of the number of coil turns on the electromagnetic force at different driving currents are primarily determined by the effects of the coil turns on the total magnetic flux and the total magnetic reluctance.

Acknowledgments

This work is supported by the National Natural Science Foundation of China (Grant No: 51475100), the Natural Science Foundation of Heilongjiang Province of China (Grant No: LC201422), the China Scholarship Council (Grant No: 201506685031), the Fundamental Research Funds for the Central Universities (Grant No: HEUCFM170302).

References

[1] L.W. Su, X.R. Li, Z. Zhang et al., Numerical analysis on the combustion and emission characteristics of forced swirl combustion system for DI diesel engines, *Energy Conversion & Management* **86** (2014), 20–27. Doi: 10.1016/j/enconman.2014.05.023.
[2] L.W. Su, X.R. Li, X. He et al., Experimental research on the diffusion flame formation and combustion performance of forced swirl combustion system for DI diesel engines, *Energy Conversion & Management* **106** (2015), 826–834. Doi: 10.1016/j.enconman.2015.10.027.
[3] X.R. Wang, M.M. Zhu, C.P. Liu et al., Effect of the fuel injector parameters on combustion performance and emissions in a marine diesel, *Journal of Computational and Theoretical Nanoscience* **12** (2015), 2897–2902. Doi: 10.1166/jctn.2015.4196.
[4] X.R. Li, H.Q. Zhou, L.W. Su et al., Combustion and emission characteristics of a lateral swirl combustion system for ID diesel engines under low excess air ratio conditions, *Fuel* **184** (2016), 672–680. Doi: 10.1016/j.fuel.2016.07.071.
[5] W. Jing, Z.Y. Wu, W.L. Roberts et al., Spray combustion of biomass-based renewable diesel fuel using multiple injection strategy in a constant volume combustion chamber, *Fuel* **181** (2016), 718–728. Doi: 10.1016/j.fuel.2016.05.039.
[6] W. Jing, W.L. Roberts and T.G. Fang, Spray combustion of Jet-A and diesel fuels in a constant volume combustion chamber, *Energy Conversion & Management* **89** (2015), 525–540. Doi: 10.1016/j.enconman.2014.10.010.

[7] Z.Y. Sun, G.X. Li, Y.S. Yu et al., Numerical investigation on transient flow and cavitation characteristic within nozzle during the oil drainage process for a high-pressure common-rail DI diesel engine, *Energy Conversion & Management* **98** (2015), 507–517. Doi: 10.1016/j.enconman.2015.04.001.
[8] Z.Y. Sun, G.X. Li, C. Chen et al., Numerical investigation on effects of nozzle's geometric parameters on the flow and cavitation characteristics within injector's nozzle for a high pressure common rail DI diesel engine, *Energy Conversion & Management* **89** (2015), 843–861. Doi: 10.1016/j.enconman.2014.10.047.
[9] Y. Bai, L.Y. Fan, X.Z. Ma et al., Effect of injector parameters on the injection quantity of common rail injection system for diesel engines, *International Journal of Automotive Technology* **17** (2016), 567–579. Doi: 10.1007/s12239-016-0057-2.
[10] Z.Y. Sun, G.X. Li, L. Wang et al., Effects of structure parameters on the static electromagnetic characteristics of solenoid valve for an electronic unit pump, *Energy Conversion & Management* **113** (2016), 119–130. Doi: 10.1016/j.enconman.2016.01.031.
[11] E.E. Topcu, I. YukseI and Z. Kamis, Development of electro-pneumatic fast switching valve and investigation of its characteristic, *Mechatronics* **16** (2006), 365–378. Doi: 10.1016/j.mechatronics.2006.01.005.
[12] S.M.A. Jaber, Energy and momentum considerations in an ideal solenoid, *Journal of Electromagnet Analysis and Applications* **2** (2010), 169–173. Doi: 10.4236/jemaa.2010.23024.
[13] Q. Cheng, Z.D. Zhang, H. Guo et al., Improved processing and performance of GDI injector based on metal injection molding technology, *International Journal of Applied Electromagnetic and Mechanics* **44** (2014), 99–114. Doi: 10.3233/JAE-131739.
[14] Q. Wang, F. Yang, Q. Yang et al., Experimental analysis of new high speed powerful digital solenoid valves, *Energy Conversion & Management* **52** (2011), 2309–2313. Doi: 10.1016/j.enconman.2010.12.032.
[15] Q.F. Liu, H.L. Bo and B.K. Qin, Experimental study and numerical analysis on electromagnetic force of direct action solenoid valve, *Nuclear Engineering & Design* **240** (2010), 4031–4036. Doi: 10.1016/j.nucengdes.2010.09.028.
[16] J.I. Miller, T.J. Flack and D. Cebon, Modeling the magnetic performance of a fast pneumatic brake actuator, *Journal of Dynamic Systems Measurement & Control* **136** (2014), ID 021022. Doi: 10.1115/1.4025813.
[17] P. Liu, L.Y. Fan, Q. Hayat et al., Research on key factor and theirs interaction effects of electromagnetic force of high speed solenoid valve, *Scientific World Journal* **5** (2014), ID567242. Doi: 10.1155/2014/567242.
[18] Q. Liu, H. Bo and B. Qin, Optimization of direct action solenoid valve based on CloudPSO, *Annals of Nuclear Energy* **53** (2013), 299–308. Doi: 10.1016/j.anucene.2012.06.028.
[19] Y.O. Shin, S.H. Lee, C.H. Choi et al., Shape optimization to minimize the response time of direct-acting solenoid valve, *Journal of Magnetics* **20** (2015), 193–200. Doi: 10.4283/JMAG.2015.20.2.193.
[20] G. Sefkat, The design optimization of the electromechanical actuator, *Structural and Multidisciplinary Optimization* **37** (2009), 635–644. Doi: 10.1007/s00158-008-0254-3.
[21] H.F. Lu, J. Deng, Z.H. Hu et al., Impact of control methods on dynamic characteristic of high speed solenoid injectors, SAE Paper, 2014-01-1445. Doi: 10.4271/2014-01-1445.
[22] F.J. Salvador, P. Marti-Aldaravi, M. Carreres et al., An investigation on the dynamic behavior at different temperatures of a solenoid operated common rail ballistic injector by means of a one dimensional model, SAE Paper, 2014-01-1089. Doi: 10.4271/2014-01-1089.
[23] F.J. Salvador, J. Gimeno, J. De la Morena at al., Using one-dimensional modeling to analyze the influence of the use of biodiesels on the dynamic behavior of solenoid-operated injectors in common rail systems: Results of the simulations and discussion, *Energy Conversion & Management* **54** (2012), 122–132. Doi: 10.1016/j.enconman.2011.10.007.
[24] R. Payri, F.J. Salvador, P. Martf-Aldaravf at al., Using one-dimensional modeling to analyze the influence of the use of biodiesels on the dynamic behavior of solenoid-operated injectors in common rail systems: Detailed injection system model, *Energy Conversion & Management* **54** (2012), 90–99. Doi: 10.1016/j.enconman.2011.10.004.